# Durability and wear resistance of laser-textured hardened stainless steel surfaces with hydrophobic properties

Garcia Giron, Antonio; Romano, Jean-Michel; Dashtbozorg, Behnam; Dong, Hanshan; Martinez-Solanas, Elena; Urrutia Angos, David; Walker, Marc; Penchev, Pavel; Dimov, Stefan

*DOI:*
10.1021/acs.langmuir.9b00398



*Document Version*
Peer reviewed version

*Citation for published version (Harvard):*
Garcia Giron, A, Romano, J-M, Dashtbozorg, B, Dong, H, Martinez-Solanas, E, Urrutia Angos, D, Walker, M, Penchev, P & Dimov, S 2019, 'Durability and wear resistance of laser-textured hardened stainless steel surfaces with hydrophobic properties', *Langmuir*, vol. 35, no. 15, pp. 5353-5363.
https://doi.org/10.1021/acs.langmuir.9b00398

# Durability and wear resistance of laser-textured hardened stainless steel surfaces with hydrophobic properties

*A. Garcia-Giron[1,*], J. M. Romano[1], A. Batal[1], B. Dashtbozorg[2], H. Dong[2], E. Martinez Solanas[3,4], D. Urrutia Angos[3,4], M. Walker[5], P. Penchev[1] and S.S. Dimov[1]*

[1]Department of Mechanical Engineering, School of Engineering, University of Birmingham, Edgbaston, Birmingham, B15 2TT, UK

[2]School of Metallurgy and Materials, University of Birmingham, Edgbaston, Birmingham, B15 2SF, UK

[3]ATRIA Innovation, C/Alaún 14, nave 5, 50197, Zaragoza, Spain

[4] Center for Corporate Technology and Innovation Spain, BSH Electrodomésticos España, S.A, Av. de la Industria 49, 50016 Zaragoza, Spain

[5]Department of Physics, University of Warwick, Coventry CV4 7AL, UK

*Corresponding author: Tel: +44 (0) 7843 859099; E-mail: antoniogarciagiron@gmail.com

**Keywords:** Laser patterning; nanosecond laser; hydrophobicity; plasma surface alloying; wear resistance; surface engineering.

ABSTRACT

Hydrophobic surfaces are of high interest to industry. While surface functionalization has attracted a significant interest, both from industry and research, the durability of engineered surfaces remains a challenge, as wear and scratches deteriorate their functional response. In this work, a cost-effective combination of surface engineering processes on stainless steel was investigated. Low temperature plasma surface alloying was applied to increase surface hardness from 172 to 305 HV. Then, near-infrared nanosecond laser patterning was deployed to fabricate channel-like patterns that enabled superhydrophobicity. Abrasion tests were carried out to examine the durability of such engineered surfaces during daily use. In particular, the evolution of surface topographies, chemical composition and water contact angle with increasing abrasion cycles were studied. Hydrophobicity deteriorated progressively on both hardened and raw stainless steel samples, suggesting that the major contributing factor to hydrophobicity was the surface chemical composition. At the same time, the samples with increased surface hardness exhibited a slower deterioration of their topographies when compared with non-treated surfaces. A conclusion is made about the durability of laser-textured hardened stainless steel surfaces produced by applying the proposed combined surface engineering approach.

## 1. Introduction

Surface functionalization technologies have attracted a significant industrial interest due to the wide range of properties that can be created on the surface. By applying chemical coatings or by modifying surface topographies at micron or sub-micron scales, surface properties can be enhanced, modified or even new ones introduced to products. For example, anti-bacterial [1], hydrophobicity [2], tribological [3] or anti-icing [4] are some of the properties that can be achieved when using such techniques.

The term wettability refers to the way a surface responds to the interaction with a liquid. In particular, when water is the liquid, the surface can be classified as hydrophilic when droplets spreads, or hydrophobic if the droplets stays rounded or are repelled. Depending on the surface response to water droplets, different wetting states can be identified, i.e. (i) the hemi-wicking state is present when the droplets spread over the surface; (ii) the Wenzel state or the homogeneous wetting regime is present when the droplets can wet the "valleys" within the surface topographies but does not spread; and (iii) the Cassie-Baxter state or heterogeneous wetting regime, when there is air trapped between the droplets and the surface, and thus, the droplets do not wet the "valleys" within the topographies [5]. Cassie-Baxter state often leads to high hydrophobicity. Water repellence is an important characteristic of hydrophobic surfaces that is closely related to corrosion resistance improvements, anti-icing, anti-fouling, liquid transportation or self-cleaning [6–10] properties. Thus, hydrophobicity is of great interest to a wide range of engineering applications, e.g. in aerospace, naval or home appliances industrial sectors, and also to many product development projects.

Different metrics can be used to quantify wettability, i.e. rolling angle, drop bouncing, hysteresis measured with the advancing and receding contact angle, or static contact angle (SCA) measurements [11]. However, SCA is the metric that is the most commonly used due its simplicity.

When SCA is smaller than 90° the surface is classified as hydrophilic, while when it is higher the surface is considered to be hydrophobic. SCA values equal or exceeding 150° are one of the main conditions for a give surface to be considered superhydrophobic [2,12], together with low roll-off angles[13]. SCA is the angle at which the liquid–vapor and solid-liquid interfaces meet.

In the case of a homogeneous wetting regime, i.e. the Wenzel state, the contact angle is calculated by using the following equation:

$$\cos\theta = r\frac{\sigma_{SV}-\sigma_{SL}}{\sigma_{LV}} \quad (1)$$

where: $r$ is the ratio of true area of the solid surface to the apparent area; and $\sigma_{SV}$, $\sigma_{SL}$ and $\sigma_{LV}$ are the surface tensions between solid-vapour, solid-liquid, and liquid-vapour interfaces, respectively, that are determined by the respective liquid, surface and air compositions.

When the surface is heterogeneous and the Wenzel model is not sufficient, the contact angle can be calculated using the Cassie-Baxter equation:

$$\cos\theta = f_1\frac{\sigma_{SV}-\sigma_{SL}}{\sigma_{LV}} - f_2 \quad (2)$$

where: $f_1$ and $f_2$ are the area fractions of solid and air in contact with the liquid, respectively.

Based on Eq.1 and Eq.2, it could be inferred that the contact angle depends on two main factors, i.e. surface chemistry and topography. Thus, if the surface energy is assumed constant, a change in topography will always lead to a change of wetting properties.

Different methods have been employed to create hydrophobic surfaces, e.g. photolithography [14], electron-beam lithography [15] or chemical coatings [16–18]. Recently, laser processing has emerged as a viable alternative for producing hydrophobic surfaces with a potential for upscaling that is a very important factor for its broader use by industry. There are two main approaches for producing superhydrophobic surfaces through laser processing. First is a two stage process that involves laser patterning/texturing to change the surface topography, i.e. for creating channels [19–21], lotus-like

patterns [22] or rose petal shapes [23], followed by a chemical non-polar coating to change the surface energy. The second approach employs only laser patterning and there are different alternatives for producing superhydrophobic surfaces depending on the scales of the generated topographies. Submicron patterns with different periodicities and distributions, like honeycomb [24] or linear [25], can be obtained by generating laser induced periodic surface structures (LIPSS). Whereas at the micro scale, direct laser interferences [26] or direct laser writing (DLW) can be deployed, with the latter being the most widely used method due to its simplicity, faster processing times and cost effectiveness; which comes as a result of the relatively low cost of nanosecond laser sources. DLW has been applied successfully to produce superhydrophobic surfaces on a wide range of metals, e.g. aluminium [27,28], stainless steel [29] and brass or copper alloys [30].

It has been widely reported that metallic surfaces are hydrophilic initially, just after laser patterning, and then they become hydrophobic with time [13,31]. However, the mechanism of this wettability evolution in time (so called aging process) is not fully understood. Some studies suggest that the contact angle changes are the result of some partial deoxidation of the laser patterned surfaces [30], while others attribute this to the presence of induced non-polar molecules on surfaces, especially due to the adsorption of organic elements from air [32,33] and inhibition of water molecules deposition [34]. Nevertheless, surface topographies produced by laser patterning remain unaltered while the wettability evolves and thus the changes in contact angle must be influenced by surface chemistry, which can be also inferred from Eq.1 and Eq.2.

Irrespective of the processing method employed, a major concern is durability of the obtained surface functionality as a result of wear and scratches that could have a progressive detrimental effect on their properties [35]. Recently, several researchers have reported investigations into the mechanical durability of hydrophobic surfaces. In most of them the surface functional response

was achieved by combining surface texturing with some chemical modifications [36–39]. Wang et al. developed a method to produce hierarchical micro-nanostructures on steel surfaces, where the microstructures behaved as a protection for the nanoscale roughness, and then a chemical etching with ultrasonic treatment was applied to modify them chemically[36,37]. Su et al. combined electrodeposition with heat-treatment in a chemical solution to fabricate cone-like microstructures on copper substrates [38]. Another approach was reported by She et al. [39], where electrodeposition followed by a chemical modification was used on magnesium alloys. Other researchers investigated laser microstructuring, especially femtosecond laser processing to create cone-like dual scale patterns on pristine metal plates [40] or surfaces with high roughness on aluminum alloys [41]. Moreover, nanosecond lasers were also employed to create hydrophobic surfaces with enhanced wear resistance by applying hydrophobic coating over channel-like patterns on stainless steel [42] or by inducing roughness on aluminum-magnesium alloyed surfaces [43]. A common aspect of all research referred to so far was that the surface topography was first modified and only then a chemical coating was applied to modify the surface energy. Particularly, patterning or other approaches were employed to create a topography or just to increase the surface roughness and thus to protect [44] and potentially to enable air trapping in the resulting topography.

However, despite the fact that hydrophobic surfaces can be produced by one-step DLW, their durability remains unstudied, especially with regards to the evolution of their topographies and respective properties due to wear and scratches. Specifically, water contact angles decrease drastically after scratching, touching or even after wetting the surfaces, due to topography changes and chemical contaminations that lead to surface tension modifications. The wear resistance of the substrate material is an important factor affecting the durability of any functionalized surface irrespective of its treatment by one-step DLW or just patterning as protection for a hydrophobic

coating. Enhancing substrates physicochemical characteristics, e.g. hardness [45], before any surface functionalization step, seems a promising approach to increase their wear resistance.

In this research, the durability and wear resistance of hydrophobic patterns on untreated and plasma treated stainless steel [46] plates produced using an infrared nanosecond laser source is investigated. The impact of substrate hardness on wear resistance and durability of hydrophobic surfaces produced by one-step DLW is analysed. Specifically, rubbing tests were conducted and the topographical evolution and accompanying chemical composition changes were studied together with their effects on surface functionality. The results from wettability and chemical analyses are reported and discussed and conclusions are made.

## 2. Materials and methods

### 2.1.Sample preparation

Circular ferritic stainless steel X6Cr17 samples were cut with a diameter and thickness of 36 and 0.7 mm, respectively. After the cutting, all plates were ground and polished to remove any oxides and contaminants. Half of the plates were hardened by DC plasma carburising, i.e. by using an adapted DC Klöckner Ionon 40 kVA plasma furnace. Samples were freshly polished to remove any residual oxides on the surfaces and also to allow atomic diffusion during the hardening process. The carburising process was performed for 20 hours at 400°C, using a mixture of 1.5% $CH_4$: 98.5% $H_2$ at 3 mbars of gas pressure. The stainless steel and plasma carburised plates were cleaned using an ultrasonic bath with ethanol.

Glow-discharge optical emission spectroscopy (GDOES) was carried out on the alloyed samples to measure depth and mass concentration of the treatment, using a Spectruma GDA 650HR analyser. Hardened layers of 1 μm thickness were obtained, with a C mass concentration of 12.9% at the surface.

Hardness was measured using a Mitutoyo MVK-H1 micro-hardness tester with a diamond Vicker's indenter; the load was set at 500 gf for the analysis. Measured hardness of as-received and plasma carburised stainless steel samples were 172 HV and 305 HV, respectively.

### 2.2.Laser processing

A laser micromachining system was used to produce the surface patterns that integrates a MOPA-based Yb-doped fibre nanosecond (ns) laser source (SPI G4 50W HS-S) with a near infrared wavelength (1064 nm) and a maximum average power of 50 W and a 100 mm telecentric focusing lens for achieving a beam spot size of 35 μm. The laser beam movements were controlled employing a 3D scan head (RhoThor RTA) and thus to be able to produce predefined patterns. A maximum scanning speed of 2.5 m/s can be achieved with the used laser processing setup.

Channel-like patterns were created on the sample surfaces. The distance between scan lines was set at 100 μm. This laser processing strategy was chosen over other possible patterns, e.g. cell-like or dimples' patterns, due to the higher anisotropy of the resulting topographies. This is important in order to be able to study how the wear directionality in respect to the pattern orientation can affect the functionality in the laser processed surfaces.

The pulse durations used to produce the patterns were 15 and 220 ns, the lowest and the highest achievable with this particular laser source and thus to judge about the trade-offs between speed

and quality in producing the patterns and their impact on wear resistance. The other processing parameters were chosen in order to maintain the same accumulated energy per line based on previous experimental results [46] as follows:

- 220 ns: scanning speed of 150 mm/s, pulse frequency of 70 kHz and pulse energy of 50.1 µJ.
- 15 ns: scanning speed of 132 mm/s, pulse frequency of 100 kHz and pulse energy of 30.9 µJ.

### 2.3. Hydrophobic coating

Two of the plasma carburised samples patterned with the 220 ns laser pulses were coated by immersion in Mecasurf® (Surfactis, Angers, France), a hydrophobic monolayer coating commercially used in aeronautics to reduce surface tension. This was done in order to compare the durability of naturally aged samples against the coated ones.

### 2.4. Abrasion test

Abrasion tests were performed on the samples to study the behaviour of the patterns under heavy wear conditions and thus to analyse any changes in functionality, chemistry and surface topography. The test was specially designed to be able to study the mechanical durability of the engineered surfaces in conditions as close as possible to those they could be exposed to in a real working environment. As there is not a standardised method to measure the durability of patterned/textured surfaces, all tests were performed by adapting the ISO 11998:2006 “Paints and varnishes – Determination of wet-scrub resistance and cleanability of samples” [47], used to test the resistance of coated surfaces. An Elcometer 1720 Abrasion and Washability Tester was used for this purpose. The test setup includes a moving mechanical arm with a counterpart holder and a load as shown in Fig.1 (a) to perform reciprocating movements on a surface and thus to induce a

tangential abrasion. Dimensions of the counterpart holder used were 90 x 39 mm, and a cadence of 37 cycles per minute was kept constant during the tests. A total stroke length of 180 mm with a load of 0.05 kgf/cm$^2$ was used, and the number of cycles performed were 100, 200 and 300.

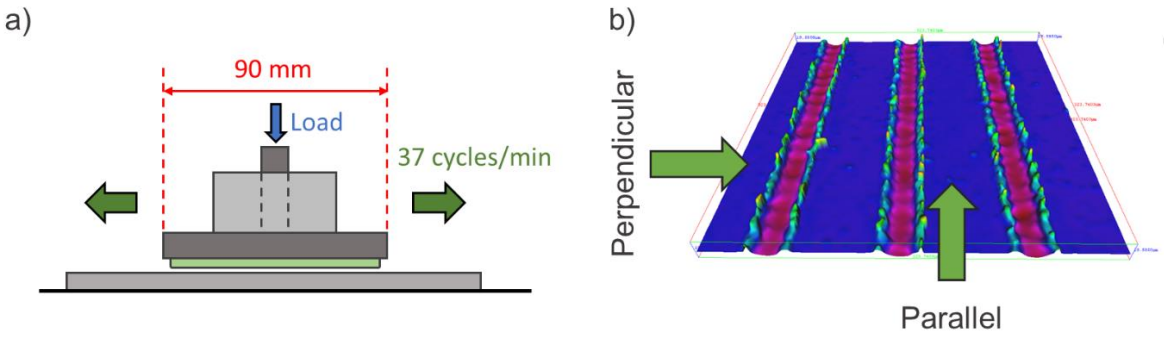


**Fig 1.** (a) a sketch of the Elcometer 1720 Abrasion and Washability Tester. (b) the relative orientation between the two abrasion directions and channel-like patterns.

Commercially available heavy-duty scouring pads (Scotch-Brite$^{TM}$) were used as counterparts during the tests. The composition of the pad in percentage weight was given by the manufacturer: aluminium oxide (45-67%), cured resin (15-40%), nylon fiber (5-15%) and titanium oxide (0.5-2.75%). The scouring pads are chemically stable and therefore it was considered that no chemical interactions between the pads and engineered surfaces took place in the tests. Counterparts were replaced after each 100 cycles to avoid the build-up of stainless steel particles during the cycles and thus to minimise their potential contribution to wear in subsequent cycles.

As is shown in Fig.1 (b), the relative orientations between the channel-like patterns and reciprocating movements were varied, i.e. they were parallel and perpendicular to the channels. After the tests, the samples were rinsed with water and dried with compressed air to remove all debris on their engineered surfaces and fibers from the scouring pads.

## 2.5.Characterization methods

A focus variation microscope, Alicona G5, with a 20x magnification lens was used to analyse the topographies of the engineered surfaces, before and after the wear cycles. The vertical resolution of the system is 50 nm. In particular, the initial depth of the channel, the height of the bulges resulting from the redeposited material after the laser patterning and then their changes after the abrasion tests were measured to quantify the wear. Uncertainty of the measurements was calculated based on the standard deviation of 10 consecutive measurements in different areas of the patterned surfaces and it was less than 0.6 μm in all cases.

A JEOL JCM-6000 Benchtop Scanning Electron Microscope (SEM) was used to obtain the micrographs of the produced patterns before and after the abrasion tests.

Wettability of the surfaces was studied using a sessile drop technique and thus to obtain their respective SCAs, with an Attension Biolin Scientific Theta T2000-Basic+ contact angle measurement system employed for these measurements. Milli-Q water droplets of 6 μl were used for all SCA measurements.

X-Ray photoelectron spectroscopy (XPS) measurements were performed on both, stainless steel and plasma carburised surfaces. The reference surfaces were analysed prior to patterning them and also on a "freshly" laser processed samples (within the 24 hour time period before the surfaces become hydrophobic), "aged" laser patterned surfaces (i.e. when the surface is hydrophobic) and "aged" surfaces after undergoing 300 wear cycles. A Kratos Axis Ultra DLD spectrometer (Kratos Analytical, UK) with a monochromated Al Kα X-ray irradiation source was used for the XPS analysis. Analysis areas of 300 x 700 μm were scanned at room temperature under a base pressure

of 2 x $10^{-10}$ mbar and the estimated depth of the XPS analysis was 5-10 nm. The measurements were calibrated by using the Fermi edge and $3d_{5/2}$ peak recorded from a polycrystalline Ag sample. Data analysis was carried out with the CasaXPS package.

## 3. Results and discussion

### 3.1. Surface analysis

Laser patterning in the nanosecond regime is a thermal process. In particular, the substrate material is molten as a result of the irradiation with nanosecond laser pulses and pulse trains lead to splashes of molten material that then solidify to create bulges on the surface. The increase of pulse duration leads to bigger volumes of molten material and thus to bigger bulges along the laser path. Therefore, two different pulse durations, i.e. 15 ns and 220 ns, were used to investigate how they could affect the wear resistance of laser functionalised surfaces. As shown in Fig. 2 (a), the obtained topographies with 15 ns pulses were well defined patterns with small volumes of solidified material along the trenches; whereas when the patterning was performed with 220 ns pulses, relatively big bulges were formed along the trenches and therefore they were less well defined (see Fig. 2 (e)). Therefore, the tribological contacts between the counterpart and the patterned areas were different when the abrasion tests were performed.

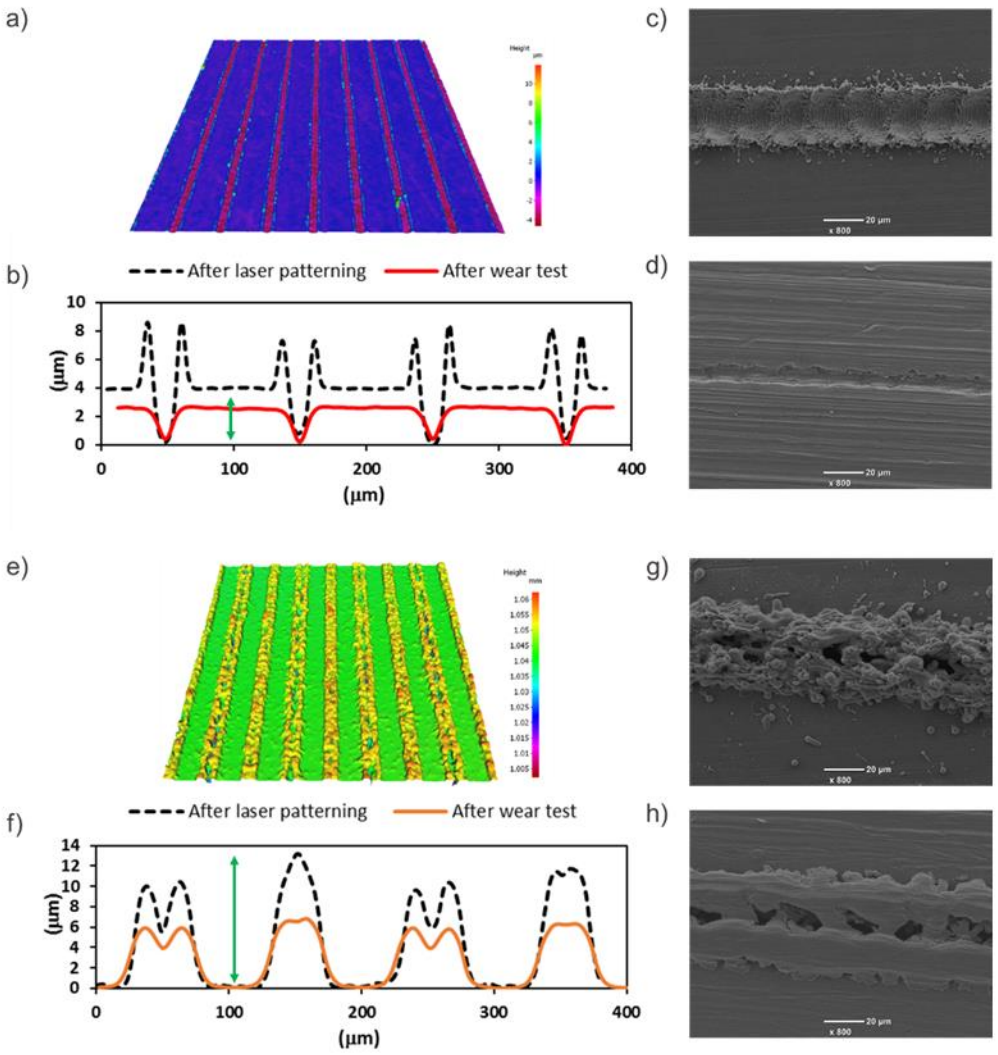


**Fig 2.** 3D images of patterns produced with pulse durations of 15 ns (a) and 220 ns (e); topographical profiles resulting after irradiation with 15 ns (b) and 220 ns (f) pulses before and after the wear tests (300 abrasion cycles); SEM images of the topographies produced with 15 ns and 220 ns before (c & g) and after (d & h) the wear tests, respectively.

Fig. 2 (b) shows representative profiles of the patterns produced with 15 ns pulses, the black dashed line before and the red line after the abrasion tests. The size of the resulting bulges could be considered negligible, i.e. only 1.1 and 1.8 µm on as-received and carburised stainless steel sample,

respectively, in comparison with the channels' width of 100 µm. Furthermore these bulges were thin and brittle, were removed quickly at the start of the abrasion tests and thus the non-processed surface was in a tribological contact with the counterpart. Then, due to the wear during the abrasion cycles the depth of the channels was reduced, as depicted in Fig 2 (b) and Fig S1. Fig. 2 (c) and (d) show the SEM images of the 15 ns topographies before and after the wear tests, respectively, clearly demonstrating the removal of the bulges and the reduction in the depth of the channels.

Fig 2. (f) shows representative profiles of the patterns produced with 220 ns pulses where the black dashed and orange lines represent the profiles before and after the abrasion tests, respectively. In this case, the bulges are in a tribological contact with the counterpart and thus the resulting abrasion had reduced their size. The height reduction of these bulges as a result of the wear can be clearly seen in Fig 2 (f) and Fig S2. Fig. 2 (g) and (h) show the SEM images of the 220 ns patterns before and after the abrasion tests. It can be clearly seen that first, the channels are almost buried under the bulges and there is a high amount of splashes and a relatively high roughness on the patterned surfaces. After the abrasion tests, the pattern is still visible on the surface, however, the bulges are smoother and as a result the surface roughness is reduced.

Fig. 3 depicts the impact of wear on the dimensions of the pattern with the increase of abrasion cycles. In particular, the depth changes of the channels produced with the 15 ns pulses are plotted in Fig. 3 (a) while in Fig. 3 (b) the height evolution of the bulges generated with the 220 ns pulses is shown. In both graphs, the profile of the pattern changes on the plasma carburised and as-received stainless steel samples are represented. Furthermore, the continuous and dashed lines depict the results obtained by performing the wear tests with abrasion directions parallel and perpendicular to the patterns, respectively.

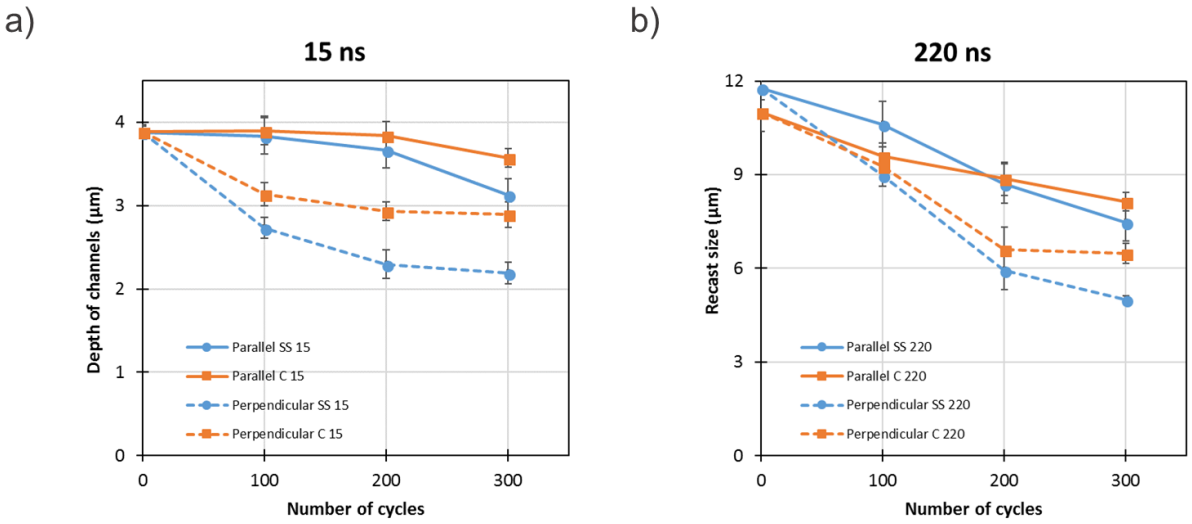


**Fig 3.** Topography and bulges' evolutions after abrasion cycles: (a) the depth changes of the channels produced with 15 ns pulses after 100, 200 and 300 cycles; (b) the height changes of the bulges generated with 220 ns pulses after 100, 200 and 300 cycles.

As can be seen in Fig. 3 (a), the depth of 15 ns channels is the same both on as-received and plasma carburised stainless steel samples, i.e. 3.9 µm deep, before the abrasion tests. Whereas in case of 220 ns patterns (see Fig. 3(b)), the height of the bulges is slightly higher on the as-received sample, i.e. 11.8 µm, compared to that on the carburised steel one, i.e. 11.0 µm**.** This height difference could be explained with the lower ablation threshold of as-received stainless steel at this pulse duration [46] and thus a bigger volume of material is melted and splashed on the surface.

The total reduction, *R,* represents the decrement in the size of the patterns after the abrasion tests in percentages and was calculated with the following equation:

$$R\ (\%) = \frac{X_i - X_f}{X_i} * 100 \qquad (3)$$

where: $X_i$ is the initial value of channel depth or bulge height obtained for the 15 ns or 220 ns patterns, and $X_f$ - their final values after 300 abrasion cycles. Table 1 includes the values of R calculated for the patterned samples after the wear tests.

Table 1. The total reductions (R) after 300 parallel and perpendicular abrasion cycles.

| | R after 300 cycles | |
|---|---|---|
| | Parallel | Perpendicular |
| SS 220 ns | 36.4 | 57.4 |
| C 220 ns | 26.1 | 41.1 |
| SS 15 ns | 19.4 | 43.4 |
| C 15 ns | 8.0 | 25.5 |

Note: SS and C denote as-received (Stainless steel) and carburised stainless steel samples respectively, while 220 and 15 ns the pulse durations used to produce them.

Similar trends can be observed for both graphs in Fig. 3. Especially, the wear rates, i.e. R in Table 1, are consistently higher on the as-received stainless steel samples in comparison to the plasma carburised ones and quantify the effects of the abrasion cycles on surface topography.

The effects of the orientation of the patterns with regards to the abrasion direction are also depicted in Fig. 3. The wear rates were constantly higher for all tests when the abrasion direction was perpendicular to the patterns compared to when the abrasion direction was parallel to them (dashed and continuous lines in Fig. 3, respectively). In particular, the applied forces are along the channels in the case of the parallel abrasion and thus the surface works under compression. At the same time, when a perpendicular abrasion is performed, the forces induce a tangential/tensile stress on the bulges generated with the 220 ns pulses that lead to flexion and a higher wear.

In the case of the 15 ns patterns on plasma carburised surfaces, the depth reduction of the channels after the abrasion cycles is less than 1 μm for both the parallel and the perpendicular abrasion. As the thickness of the carbon layer after the plasma treatment is approximately 1 μm, this means that during all abrasion cycles this harder layer and not the as-received stainless steel is in a tribological contact with the counterpart. The effect of this carbon layer is quantified in Table 1, in particular R is reduced from 19.4 % to 8.0 % and from 43.4 % to 25.5 % when the abrasion was parallel and perpendicular to the patterns, representing corresponding improvements of 59 % and 41 %.

For the 220 ns patterns, the pattern wear was assessed again using R. In particular, R was reduced from 36.4 % to 26.1 % and from 57.4 % to 41.1 % when parallel and perpendicular abrasion cycles were performed, respectively, representing an improvement of 28 % in both cases.

The higher improvement in wear resistance of 15 ns patterns in comparison with the 220 ns ones can be attributed to the specific tribological conditions between counterpart and functionalised surfaces. First, the contact area on the 15 ns surfaces is significantly bigger as can be clearly judged in Fig. 2, and thus the applied force is better distributed and hence the exerted pressure is lower. Secondly, the contact occurs predominantly on the bulges in the case of 220 ns patterns, both on as-received and plasma carburised stainless steel samples. The bulges are recasts mainly formed of iron oxides (see the results in Section 3.3) and therefore, the tribological contact with the hardened non-patterned carburised surface is reduced substantially and hence the wear is higher when compared with the 15 ns samples.

3.2.Wettability

SCA measurements were carried out to quantify the wettability of the patterned surfaces and also to analyse their evolution as a result of the abrasion cycles. SCAs measured on as-received and plasma carburised stainless steel samples were 92° and 98°, respectively, before the laser patterning.

It is well known that laser patterned metallic surfaces are hydrophilic just after the processing and with time they become hydrophobic due to an aging process that leads to changes in surface chemistry while their topography remains unaltered. All samples were analysed after the laser patterning and all of them exhibited high hydrophilicity. After 10 days, the samples were analysed again and then SCAs were closer to 170° while the rolling angles were low [46], indicating a transition to Cassie-Baxter state. SCAs for all samples before the laser patterning (used as references) and after 10 days following their processing are shown in Fig. 4.

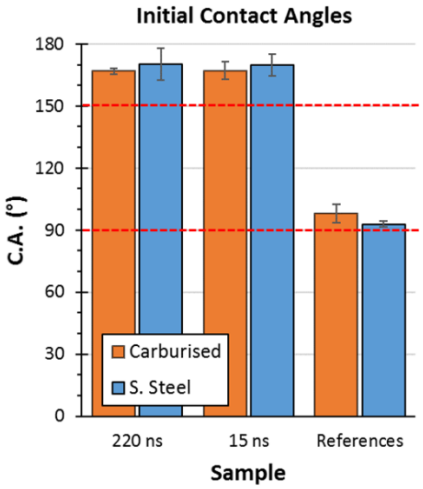


**Fig 4.** SCAs of the reference and patterned samples after 10 days stabilization.

Following the 10 day stabilization, patterned samples were used to analyse their wear resistance, with SCAs measured on the samples after undergoing 300 abrasion cycles and then cleaning them to remove any debris. Fig. 5 shows the SCA evolution with the increase of abrasion cycles. SCAs dropped from 170° to values in the range from 100° to 110° after the first 100 parallel abrasion cycles as shown in Fig. 5 (a) and were between 95° and 105° at the end of the tests, similar to the values obtained with the reference samples. This demonstrates a quick loss of hydrophobicity, regardless of the laser and plasma treatments of the four analysed samples that underwent parallel abrasions cycles. In addition, it is worth noting that on all four samples the droplets spread along the channels and became elongated following the parallel abrasion cycles (See Fig. S3).

In the case of the abrasion cycles that were performed perpendicular to the channels, the SCA decrease was not so sharp and the change of the wetting properties was progressive as can be seen in Fig. 5 (b). The patterns were continuously eroded and SCAs decreased following the Wenzel model. SCAs remained higher during the first 200 cycles on the 220 ns samples, due to the relatively higher aspect ratio of the patterns compared to those produced with 15 ns pulses. After 300 cycles, SCA values were in the range from 100° to 110°, slightly higher than the references.

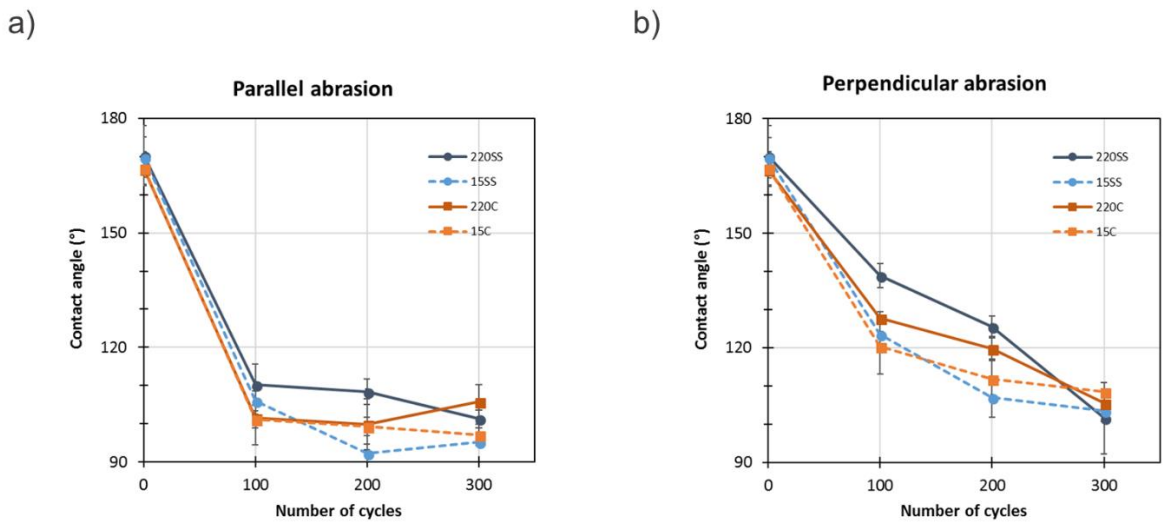


**Fig 5.** SCA evolution after 100, 200 and 300 parallel (a) and perpendicular (b) abrasion cycles.

As discussed in Section 3.1, and considering the evolution of surface topographies, the impact of wear is higher when the abrasion cycles were performed perpendicular to the channels. However, when the functional response of the surfaces was analysed, the patterns that underwent abrasion cycles perpendicular to the channels have shown a slow deterioration of their hydrophobicity. Fibers from the scouring pads used for the abrasion cycles were retained inside the channels during the tests when the reciprocating movement of the counterpart was parallel to the channels. Therefore, the fibers eroded the channels from inside and thus their surface chemistry was modified. In the case of the perpendicular abrasion, the bulges prevented the pad fibers from being deposited inside the channels, inhibiting them from wearing the channels from inside, and thus their surface chemistry was altered at much slower rate.

### 3.3.Chemical analysis

X-Ray photoelectron spectroscopy (XPS) analysis was performed on the samples to analyse the surface chemical compositions at different stages of the aging process and after the abrasion cycles. Similar trends in composition changes were obtained for the samples patterned with both pulse durations as shown in Fig. S4. However, differences in chemical compositions were bigger for the 220 ns samples due to the larger patterns (the increased surface damage due to the longer pulse duration) and therefore only the results for 220 ns samples are presented below. As-received and plasma carburised stainless steel samples were compared. Measurements were taken on all samples before any laser processing in order to use them as references. Then, measurements were taken on freshly patterned samples while they were still hydrophilic and also on aged samples, when they were super hydrophobic. Finally, the last set of measurements were taken after the wear tests, when the samples lost their hydrophobicity.

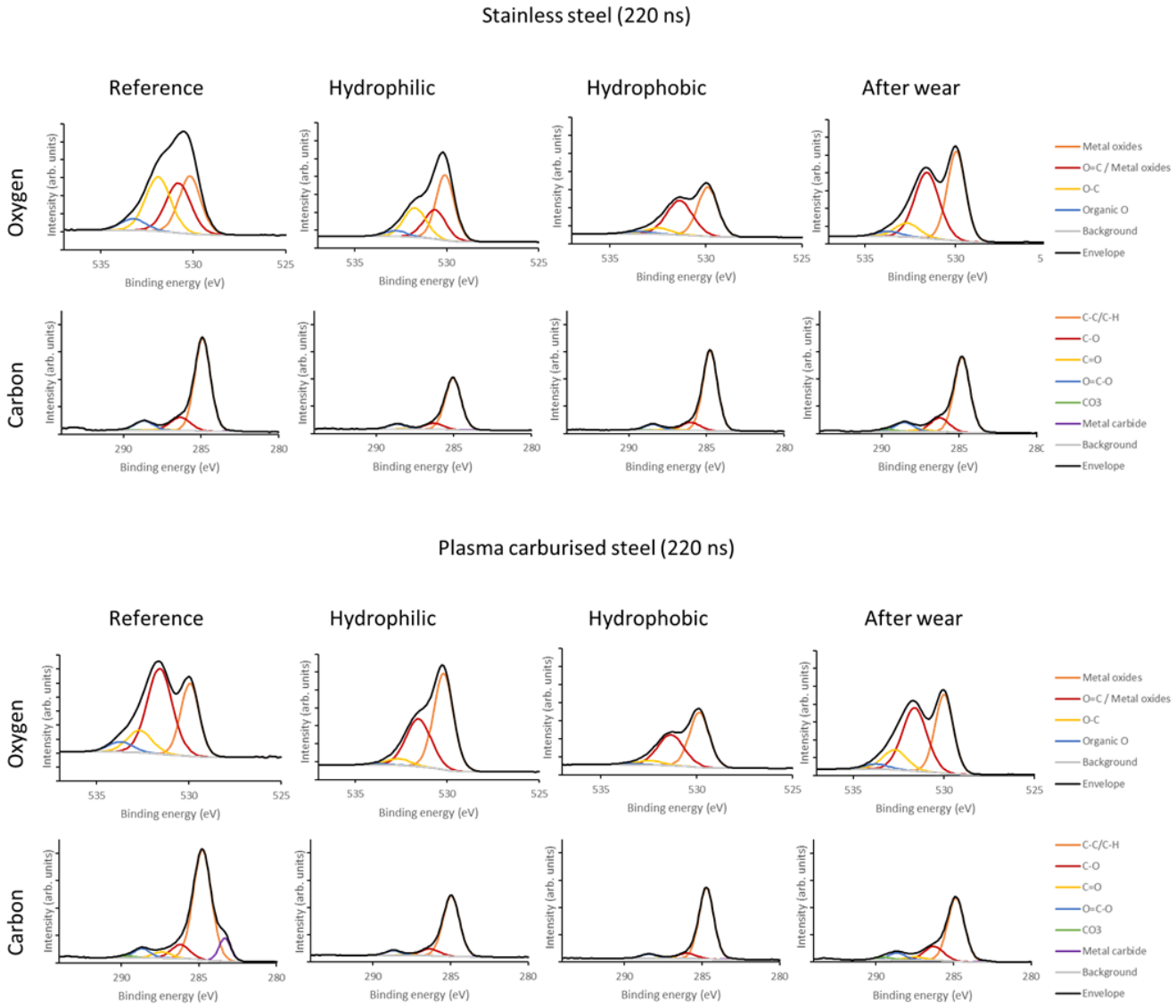


**Fig 6.** Deconvolution of the carbon (C 1s) and oxygen (O 1s) regions of as-received and plasma carburised samples patterned with 220 ns laser pulses.

Note: reference – the measurements on the samples before patterning, hydrophilic – the set of measurement taken on the "freshly" patterned samples, hydrophobic – the measurements after stabilization and wear tests – the set of measurements after 300 abrasion cycles.

After comparing the XPS survey spectra of the samples, differences were identified in the peaks corresponding to carbon and oxygen. Deconvolution of the C 1*s* and O 1*s* regions are depicted in Fig. 6, including measurements taken on the sample before and after the laser patterning and also after the wear tests. The reference measurements on as-received and plasma carburised stainless steel showed differences in their oxygen peaks. While the component corresponding to metal oxides at 530 eV were the same, there was a shift in the O=C/Metal oxide peaks from 530.8 to 531.6 eV and also in the peaks corresponding to O-C, from 531.9 to 532.7 eV, respectively. These shifts are most likely due to a change in the surface potential due to the carburisation process, with two components arising from metal oxides due to the different metal oxides present on stainless steel. The intensity of the O-C peak was higher on as-received stainless steel, while the O=C/metal oxide peak was higher on plasma carburised surface. These differences in oxidation states can be attributed to the high amount of carbon present on the plasma carburised samples before the laser processing. A peak at 533.5 eV can be identified on both samples, corresponding to organic oxygen, possibly enhanced by water molecules on the surface. Considering the carbon peaks on as-received and plasma carburised reference samples, this could be explained with the high amounts of surface contaminants due to the C-O, O=C-O and C-C/C-H bonds. In the case of plasma carburised stainless steel, the C-C/C-H peak is higher due to the carbon alloying process. Additionally, a peak at 283.3 eV could also be observed on this sample, indicating the presence of metal carbides.

Deconvolution of the O 1*s* region after laser processing on hydrophilic as-received and carburised stainless steel samples also revealed some interesting changes as a result of the laser process. An increase in the metallic oxide component at 530 eV can be identified on both surfaces, to the detriment of the other peaks, explained by the solidification and subsequent oxidation of molten

metal during the laser patterning and the formation of bulges along the channels. For both surfaces, the C 1*s* profiles are similar but reduced in intensity compared with the references, suggesting a reduction in the concentration of surface contaminants. No carbides were observed in any of the hydrophilic samples, indicating that carbon present in the as-received and carburised stainless steel was vaporised or dissolved into the lattice.

Oxygen peaks are similar on hydrophobic as-received and carburised stainless steel samples after stabilization, indicating identical oxidation states with metallic oxide peaks at 529.9 and 531.4 eV on both samples. Comparing them with the hydrophilic samples, an overall reduction in the relative intensity of the O 1*s* region was observed due to the increase of the carbon content. In addition, there is a change in the relative ratio of the peaks at 529.9 and 531.4 eV. For the as-received sample, a shift in the peak to higher binding energy can be identified, too, i.e. from 530.6 to 531.4 eV. These differences in the oxygen peaks suggest a change in the surface potential that could be attributed to the surface activation after the laser processing, and a posterior surface contamination during the samples aging. Regarding the carbon peaks, an increase of the peak at 284.7 eV can be observed when comparing the hydrophobic with the hydrophilic sample, corresponding to the C-C/C-H bonds, while the other peaks remain constant.

After the wear tests, the relative intensity of the C 1*s* region was reduced, as the contaminants from the surface were partially removed, in particular the C-C/C-H peaks are smaller compared with those on the hydrophobic samples. Furthermore, an increase of C-O and O=C-O peaks can be observed on both as-received and plasma carburised samples. On both surfaces, the oxygen peaks are at the same positions and their relative sizes are similar compared to the hydrophobic samples, suggesting that there is no change in oxidation states or surface potential after the wear tests.

However, the intensity of all the peaks is higher, due to the total reduction in carbon-based contaminants.

Carbon-carbon (C-C) and hydrocarbon species (C-H) are known to be non-polar molecules, while carbonyl groups (C=O), carbon-oxygen (C-O) and carboxyl molecules (O=C-O) together with metal oxides, are polar. Water molecules are polar, and thus if a surface polar as well, bonds form between them, leading to hydrophilicity. Furthermore, non-polar surfaces are associated with hydrophobicity. The presence of such polar and non-polar molecules on the surfaces and the change in the oxidation states explain the SCA evolution during the stabilization.

Table 2 shows the contributions of non-polar organic molecules, metal oxides and polar organic molecules to the compositions detected on the surfaces, measured in atomic weight (%). In accordance with the results in Fig. 6, the reference surface compositions were different due to the high amount of carbon present on the alloyed material. After the laser patterning, a small reduction in organic based compounds was detected, especially on the carburised surfaces, due to the cleaning effect of the laser. Furthermore, an increase in metallic oxides was found on both as-received and carburised stainless steel samples that could explain the high hydrophilicity of the "freshly" patterned surfaces.

On both hydrophobic samples, the presence of non-polar molecules is higher in comparison with the "freshly" patterned ones, while the presence of polar molecules is smaller. In addition, as previously pointed out in Fig. 6, a difference in oxygen peaks was observed on hydrophilic and hydrophobic surfaces, indicating a change in surface potential, and as topographies remained unchanged, this clearly indicates chemically active/unstable surfaces after the laser patterning. Oxidation is followed by a chemisorption of organic non-polar molecules from the atmosphere [48],

and thus in combination with the resulting surface topography after the laser patterning leads to hydrophobicity.

After the wear tests, surfaces lost the hydrophobicity, and this can be explained with the reduction of non-polar molecules, due to material removal during the abrasion cycles. Furthermore, as the surfaces reached an equilibrium state after stabilization, no changes in chemical composition occurred, suggesting that the surfaces were not chemically active anymore, and thus this could explain why the surfaces did not recover the hydrophobicity again after some time.

Table 2. Surface compositions at the four investigated states on as-received and carburised stainless steel samples.

| | Sample | Non-polar organics | Metal oxides | Polar organics | Rest |
|---|---|---|---|---|---|
| As-received | Reference | 29.0 | 20.3 | 20.0 | 30.8 |
| | Fresh sample | 29.5 | 29.1 | 17.3 | 24.1 |
| | Aged sample | 42.7 | 27.4 | 8.4 | 21.5 |
| | After wear | 28.2 | 33.4 | 10.6 | 27.9 |
| Carburised | Reference | 41.7 | 16.9 | 11.1 | 30.2 |
| | Fresh sample | 29.4 | 41.3 | 5.7 | 23.5 |
| | Aged sample | 42.2 | 31.5 | 6.2 | 20.2 |
| | After wear | 26.4 | 32.2 | 12.4 | 29.0 |

### 3.4. Durability of coated samples

As shown in Section 3.1, the wear rates (see Table 1) are consistently higher on the as-received stainless steel samples in comparison to the plasma carburised ones. Furthermore, the progressive loss of hydrophobicity with the increase of abrasion cycles was discussed in Section 3.2. Therefore, a feasibility study was conducted to investigate the effect of a commercially available hydrophobic

monolayer coating on top of topographies resulting after laser processing on two plasma carburised stainless steel samples. Especially, the surface response of uncoated and coated carburised samples patterned with 220 ns pulses was investigated under the same wear conditions, and for both parallel and perpendicular abrasion. The reference SCA on the coated surface without laser patterning was measured, too, and it was 114°, slightly higher than the reference for an unpattern carburised sample without the coating, and the response during the wear test was studied as well.

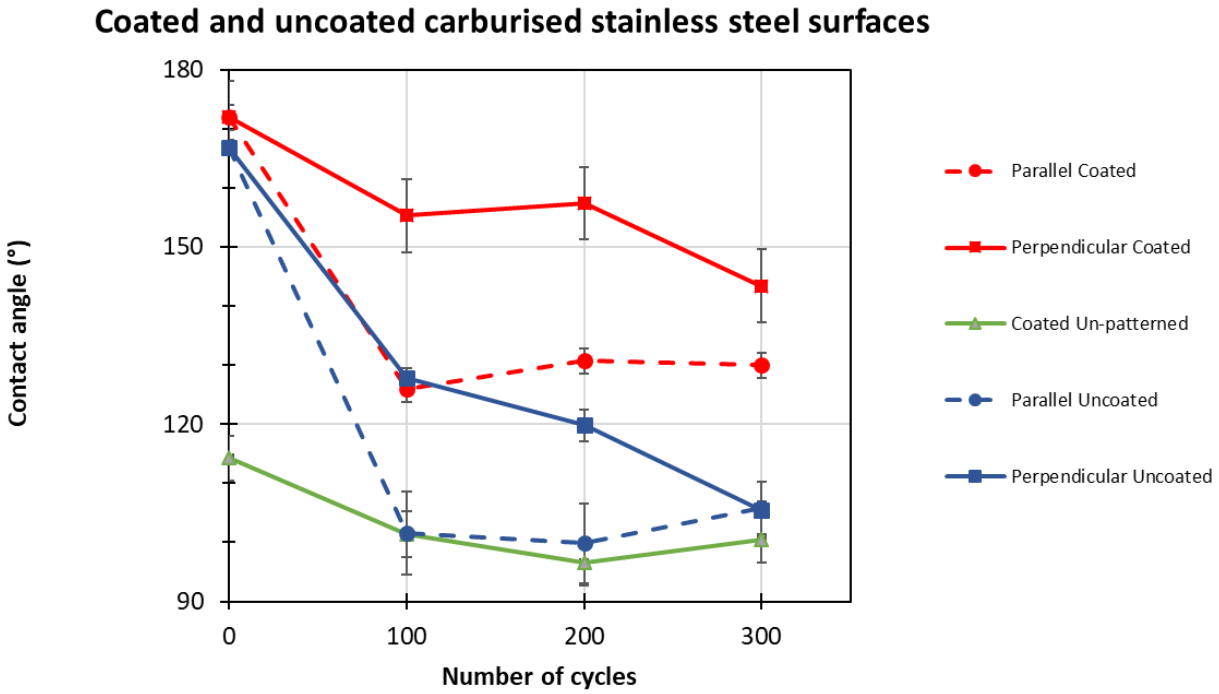


**Fig 7.** SCA evolution after 100, 200 and 300 wear cycles on uncoated and coated carburised samples patterned with 220 ns pulses, as well as the reference coated un-patterned surface.

The SCA evolution on uncoated and coated carburised 220 ns samples after perpendicular and parallel abrasion cycles is shown in Fig. 7. It can be clearly seen that the coated samples showed higher SCAs after the abrasion. This suggests that the applied coating was strongly attached to the surface not only on the bulges, as it was the case with the organic layer formed during the

stabilization, but also inside the channels and on not laser processed areas. As discussed earlier, the bulges acted like a mechanical shield for the coating. Especially, as can be clearly seen in Fig. 7, the wear of the coating is higher as a result of the parallel abrasion cycles, as the pad fibers of the counterpart got inside the channels and were progressively wearing the coating. However, when the abrasion cycles were performed perpendicular to the channels, the bulges shielded the coating and therefore SCAs were higher than 140° even after 300 cycles. Furthermore, the combination of both surface topography and coating is the key in achieving high SCAs, as can be clearly seen in Fig. 7. The coating on un-patterned surfaces is not sufficient to achieve high SCA values and thus the presence of the bulges has a double effect, i.e. increasing hydrophobicity and at the same time shielding the coating.

## 4. Conclusions

In this paper, durability, both mechanically and functionally of surface topographies produced by laser patterning was studied. Channel-like patterns were fabricated with an infrared nanosecond laser on as-received and plasma carburised stainless steel samples to investigate the evolution of their wear and wettability after abrasion cycles.

The patterns produced with longer pulse durations were more wear resistant, due to the larger volumes of melted and quenched material during the laser patterning process. Furthermore, the patterns produced on plasma treated harden surfaces showed consistently a higher wear resistance, especially a higher mechanical durability. Also, the results revealed that the abrasion cycles orientation relative to the channels was important factor affecting the surface durability. From a mechanical viewpoint, the wear resistance was higher to the parallel abrasion cycles because the

patterns were exposed to compression forces compared to the tangential stress experienced during the perpendicular abrasion cycles. However, from the wettability viewpoint, surfaces were more resistant to the perpendicular abrasion cycles. The bulges formed along the channels during the laser processing behaved as a mechanical shield, absorbing most of the abrasion, and thus inhibiting the wear by pad fibers and thus the changes of surface chemistry inside the channels. In case of the parallel abrasion cycles, pad fibers were freely moving inside the channels and thus causing a homogeneous wear along the entire surface topography. The pattern mechanical durability improvements on plasma carburised surfaces were 28 % and 59 % after laser processing with 220 and 15 ns pulses, respectively, compared to the durability achieved on as-received stainless steel substrates.

The reasons for the wettability evolution of laser patterned surfaces in time was also investigated. XPS analysis of laser patterned surfaces on as-received and carburised stainless steel samples revealed changes in their oxide peaks in time and also an increase of carbon based molecules. This suggests a surface activation after the laser processing that leads to changes in the surface potential and a chemisorption of non-polar molecules onto the surface. Furthermore, hydrophobicity attained in time could be explained with the combined effects of absorbed non-polar molecules and the topography attained after laser patterning.

In addition, it was possible by combining surface hardening, laser patterning and surface coating to retain higher hydrophobicity after wear tests, especially contact angles higher than 140° were maintained after 300 abrasion cycles by using the bulges resulting after laser patterning as a shield for the coating. Particularly, the mechanical properties were enhanced by carburizing substrates and thus to increase the wear resistance of the patterns and hence to prolong their shielding effect and protect the hydrophobic coating. Thus, the proposed combined surface treatment by first

carburizing the substrates and then laser patterning them could offer increased durability and wear resistance of functionalized surfaces that is one of the critical obstacles toward their broader use in many application areas. Further research is necessary regarding the effects of the abrasion orientation and thus propose laser patterns that could withstand heterogeneous wear cycles. Furthermore, other alloying elements should be investigated to increase even further the substrate hardness and thus the lifespan of laser-based functionalized surfaces.

## Author information

Antonio Garcia-Giron, University of Birmingham, Email: antoniogarciagiron@gmail.com

## Acknowledgements

The research reported in this paper was carried out within the framework of European Commission H2020 ITN programme "European ESRs Network on Short Pulsed Laser Micro/Nanostructuring of Surfaces for Improved Functional Applications" (www.laser4fun.eu) under the Marie Skłodowska-Curie grant agreement No. 675063 and the UKIERI DST programme "Surface functionalisation for food, packaging, and healthcare applications". In addition, the work was supported by two other H2020 FoF programmes, i.e. the projects on "Modular laser based additive manufacturing platform for large scale industrial applications" (MAESTRO) and "High-Impact Injection Moulding Platform for mass-production of 3D and/or large micro-structured surfaces

with Antimicrobial, Self-cleaning, Anti-scratch, Anti-squeak and Aesthetic functionalities" (HIMALAIA). The authors would like also to acknowledge the support and assistance of Airbus Defence and Space GmbH and B/S/H/ Hausgeräte GmbH in conducting this research.

## References

(1) Campoccia, D.; Montanaro, L.; Arciola, C. R. A Review of the Biomaterials Technologies for Infection-Resistant Surfaces. *Biomaterials* **2013**, *34* (34), 8533–8554.

(2) Bormashenko, E. Historical Perspective Progress in Understanding Wetting Transitions on Rough Surfaces. *Adv. Colloid Interface Sci.* **2015**, *222*, 92–103.

(3) Bhaduri, D.; Batal, A.; Dimov, S. S.; Zhang, Z.; Dong, H.; Fallqvist, M.; M 'saoubi, R. On Design and Tribological Behaviour of Laser Textured Surfaces. *Procedia CIRP* **2017**, *60*, 20–25.

(4) Liao, R.; Zuo, Z.; Guo, C.; Zhuang, A.; Zhao, X.; Yuan, Y. Anti-Icing Performance in Glaze Ice of Nanostructured Film Prepared by RF Magnetron Sputtering. *Appl. Surf. Sci.* **2015**, *356*, 539–545.

(5) Yu, D. I.; Doh, S. W.; Kwak, H. J.; Kang, H. C.; Ahn, H. S.; Park, H. S.; Kiyofumi, M.; Kim, M. H. Wetting State on Hydrophilic and Hydrophobic Micro-Textured Surfaces: Thermodynamic Analysis and X-Ray Visualization. *Appl. Phys. Lett.* **2015**, *106* (17).

(6) Wang, Z.; Elimelech, M.; Lin, S. Environmental Applications of Interfacial Materials with Special Wettability. *Environ. Sci. Technol.* **2016**, *50* (5), 2132–2150.

(7) Yao, X.; Song, Y.; Jiang, L. Applications of Bio-Inspired Special Wettable Surfaces. *Adv. Mater.* **2011**, *23* (6), 719–734.

(8) Jagdheesh, R.; Diaz, M.; Ocaña, J. L. Bio Inspired Self-Cleaning Ultrahydrophobic Aluminium Surface by Laser Processing. *RSC Adv.* **2016**, *6* (77), 72933–72941.

(9) Mishchenko, L.; Hatton, B.; Bahadur, V.; Taylor, J. A.; Krupenkin, T.; Aizenberg, J. Design of Ice-Free Nanostructured Surfaces Based on Repulsion of Impacting Water Droplets. *ACS Nano* **2010**, *4* (12), 7699–7707.

(10) Watson, G. S.; Green, D. W.; Schwarzkopf, L.; Li, X.; Cribb, B. W.; Myhra, S.; Watson, J. A. A Gecko Skin Micro/Nano Structure - A Low Adhesion, Superhydrophobic, Anti-Wetting, Self-Cleaning, Biocompatible, Antibacterial Surface. *Acta Biomater.* **2015**, *21*, 109–122.

(11) Bracco, G.; Holst, B. *Surface Science Techniques*; 2013; Vol. 51.

(12) Bico, J.; Thiele, U.; Quéré, D. Wetting of Textured Surfaces. *Colloids Surfaces A Physicochem. Eng. Asp.* **2002**, *206* (1–3), 41–46.

(13) Kietzig, A. M.; Hatzikiriakos, S. G.; Englezos, P. Patterned Superhydrophobic Metallic Surfaces. *Langmuir* **2009**, *25* (8), 4821–4827.

(14) Suzuki, S.; Nakajima, A.; Tanaka, K.; Sakai, M.; Hashimoto, A.; Yoshida, N.; Kameshima, Y.; Okada, K. Sliding Behavior of Water Droplets on Line-Patterned Hydrophobic Surfaces. *Appl. Surf. Sci.* **2008**, *254*, 1797–1805.

(15) Li, X.; Shao, J.; Ding, Y.; Tian, H. Microbowl-Arrayed Surface Generated by EBL of Negative-Tone SU-8 for Highly Adhesive Hydrophobicity. *Appl. Surf. Sci.* **2014**, *307*, 365–371.

(16) Bayer, I. S. On the Durability and Wear Resistance of Transparent Superhydrophobic Coatings.

(17) Cohen, N.; Dotan, A.; Dodiuk, H.; Kenig, S. Materials and Manufacturing Processes

Superhydrophobic Coatings and Their Durability Superhydrophobic Coatings and Their Durability. **2016**.

(18) Abdulhussein, A. T.; Kannarpady, G. K.; Wright, A. B.; Ghosh, A.; Biris, A. S. Current Trend in Fabrication of Complex Morphologically Tunable Superhydrophobic Nano Scale Surfaces. *Appl. Surf. Sci.* **2016**, *384*, 311–332.

(19) Emelyanenko, A. M.; Shagieva, F. M.; Domantovsky, A. G.; Boinovich, L. B. Nanosecond Laser Micro- and Nanotexturing for the Design of a Superhydrophobic Coating Robust against Long-Term Contact with Water, Cavitation, and Abrasion. *Appl. Surf. Sci.* **2015**, *332*, 513–517.

(20) Boinovich, L. B.; Emelyanenko, A. M. The Behaviour of Fluoro- and Hydrocarbon Surfactants Used for Fabrication of Superhydrophobic Coatings at Solid/Water Interface. *Colloids Surfaces A Physicochem. Eng. Asp.* **2015**, *481*, 167–175.

(21) Boinovich, L. B.; Emelyanenko, A. M.; Modestov, A. D.; Domantovsky, A. G.; Emelyanenko, K. A. Synergistic Effect of Superhydrophobicity and Oxidized Layers on Corrosion Resistance of Aluminum Alloy Surface Textured by Nanosecond Laser Treatment. *ACS Appl. Mater. Interfaces* **2015**, *7* (34), 19500–19508.

(22) He, H.; Qu, N.; Zeng, Y. Lotus-Leaf-like Microstructures on Tungsten Surface Induced by One-Step Nanosecond Laser Irradiation. *Surf. Coat. Technol.* **2016**, *307*, 898–907.

(23) Liu, Y.; Liu, J.; Li, S.; Zhiwu, H.; Yu, S.; Ren, L. Fabrication of Biomimetic Super-Hydrophobic Surface on Aluminum Alloy. *J. Mater. Sci.* **2014**, *49*, 1624–1629.

(24) Romano, J.-M.; Garcia-Giron, A.; Penchev, P.; Dimov, S. Triangular Laser-Induced Submicron Textures for Functionalising Stainless Steel Surfaces. *Appl. Surf. Sci.* **2018**, *440*.

(25) Zhang, Y.; Zou, G.; Liu, L.; Zhao, Y.; Liang, Q.; Wu, A.; Zhou, Y. N. Time-Dependent

Wettability of Nano-Patterned Surfaces Fabricated by Femtosecond Laser with High Efficiency. *Appl. Surf. Sci.* **2016**, *389*, 554–559.

(26) Alamri, S.; Aguilar-Morales, A. I.; Lasagni, A. F. Controlling the Wettability of Polycarbonate Substrates by Producing Hierarchical Structures Using Direct Laser Interference Patterning. *Eur. Polym. J.* **2018**, *99*, 27–37.

(27) Jagdheesh, R.; Garcia-Ballesteros, J. J.; Ocaña, J. L. One-Step Fabrication of near Superhydrophobic Aluminum Surface by Nanosecond Laser Ablation. *Appl. Surf. Sci.* **2016**, *374*, 2–11.

(28) Ocan??, J. L.; Jagdheesh, R.; Garci??-Ballesteros, J. J. Direct Generation of Superhydrophobic Microstructures in Metals by UV Laser Sources in the Nanosecond Regime. *Adv. Opt. Technol.* **2016**, *5* (1), 87–93.

(29) Ta, V. D.; Dunn, A.; Wasley, T. J.; Li, J.; Kay, R. W.; Stringer, J.; Smith, P. J.; Esenturk, E.; Connaughton, C.; Shephard, J. D. Laser Textured Superhydrophobic Surfaces and Their Applications for Homogeneous Spot Deposition. *Appl. Surf. Sci.* **2016**, *365*, 153–159.

(30) Ta, D. V.; Dunn, A.; Wasley, T. J.; Kay, R. W.; Stringer, J.; Smith, P. J.; Connaughton, C.; Shephard, J. D. Nanosecond Laser Textured Superhydrophobic Metallic Surfaces and Their Chemical Sensing Applications. *Appl. Surf. Sci.* **2015**, *357*, 248–254.

(31) Bizi-Bandoki, P.; Valette, S.; Audouard, E.; Benayoun, S. Time Dependency of the Hydrophilicity and Hydrophobicity of Metallic Alloys Subjected to Femtosecond Laser Irradiations. *Appl. Surf. Sci.* **2013**, *273*, 399–407.

(32) Long, J.; Zhong, M.; Zhang, H.; Fan, P. Superhydrophilicity to Superhydrophobicity Transition of Picosecond Laser Microstructured Aluminum in Ambient Air. *J. Colloid Interface Sci.* **2015**, *441*, 1–9.

(33) Boinovich, L. B.; Emelyanenko, A. M.; Emelyanenko, K. A.; Domantovsky, A. G.; Shiryaev, A. A. Comment on "Nanosecond Laser Textured Superhydrophobic Metallic Surfaces and Their Chemical Sensing Applications" by Duong V. Ta, Andrew Dunn, Thomas J. Wasley, Robert W. Kay, Jonathan Stringer, Patrick J. Smith, Colm Connaughton, Jonathan D. Shephard (Ap. *Appl. Surf. Sci.* **2016**, *379*, 111–113.

(34) Huerta-Murillo, D.; García-Girón, A.; Romano, J. M.; Cardoso, J. T.; Cordovilla, F.; Walker, M.; Dimov, S. S.; Ocaña, J. L. Wettability Modification of Laser-Fabricated Hierarchical Surface Structures in Ti-6Al-4V Titanium Alloy. *Appl. Surf. Sci.* **2019**, *463*, 838–846.

(35) Scarratt, L. R. J.; Steiner, U.; Neto, C. A Review on the Mechanical and Thermodynamic Robustness of Superhydrophobic Surfaces. *Adv. Colloid Interface Sci.* **2017**, *246*, 133–152.

(36) Wang, P.; Yao, T.; Sun, B.; Ci, T.; Fan, X.; Han, H. Fabrication of Mechanically Robust Superhydrophobic Steel Surface with Corrosion Resistance Property.

(37) Wang, N.; Xiong, D.; Deng, Y.; Shi, Y.; Wang, K. Mechanically Robust Superhydrophobic Steel Surface with Anti- Icing, UV-Durability, and Corrosion Resistance Properties.

(38) Su, F.; Yao, K. Facile Fabrication of Superhydrophobic Surface with Excellent Mechanical Abrasion and Corrosion Resistance on Copper Substrate by a Novel Method. *ACS Appl. Mater. Interfaces* **2014**, *6* (11), 8762–8770.

(39) She, Z.; Li, Q.; Wang, Z.; Li, L.; Chen, F.; Zhou, J. Researching the Fabrication of Anticorrosion Superhydrophobic Surface on Magnesium Alloy and Its Mechanical Stability and Durability. *Chem. Eng. J.* **2013**, *228*, 415–424.

(40) Han, J.; Cai, M.; Lin, Y.; Liu, W.; Luo, X.; Zhang, H.; Wang, K.; Zhong, M. Comprehensively Durable Superhydrophobic Metallic Hierarchical Surfaces via Tunable

Micro- Cone Design to Protect Functional Nanostructures. *RSC Adv.* **2018**, *8*, 6733–6744.

(41) Tang, M.-K.; Huang, X.-J.; Guo, Z.; Yu, J.-G.; Li, X.-W.; Zhang, Q.-X. Fabrication of Robust and Stable Superhydrophobic Surface by a Convenient, Low-Cost and Efficient Laser Marking Approach. *Colloids Surfaces A Physicochem. Eng. Asp.* **2015**, *484*, 449–456.

(42) Emelyanenko, A. M.; Shagieva, F. M.; Domantovsky, A. G.; Boinovich, L. B. Nanosecond Laser Micro- and Nanotexturing for the Design of a Superhydrophobic Coating Robust against Long-Term Contact with Water, Cavitation, and Abrasion. *Appl. Surf. Sci.* **2015**, *332*, 513–517.

(43) Boinovich, L. B.; Emelyanenko, K. A.; Domantovsky, A. G.; Emelyanenko, A. M. Laser Tailoring the Surface Chemistry and Morphology for Wear, Scale and Corrosion Resistant Superhydrophobic Coatings. *Langmuir* **2018**, *34*, 14.

(44) Verho, T.; Bower, C.; Andrew, P.; Franssila, S.; Ikkala, O.; Ras, R. H. A. Mechanically Durable Superhydrophobic Surfaces. *Adv. Mater.* **2011**, *23* (5), 673–678.

(45) Milionis, A.; Loth, E.; Bayer, I. S. Recent Advances in the Mechanical Durability of Superhydrophobic Materials. *Adv. Colloid Interface Sci.* **2016**, *229*, 57–79.

(46) Garcia-Giron, A.; Romano, J. M.; Liang, Y.; Dashtbozorg, B.; Dong, H.; Penchev, P.; Dimov, S. S. Combined Surface Hardening and Laser Patterning Approach for Functionalising Stainless Steel Surfaces. *Appl. Surf. Sci.* **2018**, *439*, 516–524.

(47) Standard, I. ISO 11998:2006 “Paints and Varnishes – Determination of Wet-Scrub Resistance and Cleanability of Samples.” **1998**, *1998*.

(48) Cardoso, J. T.; Garcia-Girón, A.; Romano, J. M.; Huerta-Murillo, D.; Jagdheesh, R.; Walker, M.; Dimov, S. S.; Ocaña, J. L. Influence of Ambient Conditions on the Evolution

of Wettability Properties of an IR-, Ns-Laser Textured Aluminium Alloy. *RSC Adv.* **2017**, *7* (63).